Journal of Power Sources 232 (2013) 187–192

Contents lists available at SciVerse ScienceDirect

Journal of Power Sources

journal homepage: www.elsevier.com/locate/jpowsour

Electrochemical conversion of H_2O/CO_2 to fuel in a proton-conducting solid oxide electrolyser

Guojian Wu [a], Kui Xie [a,b,c,*], Yucheng Wu [a,b,*], Weitang Yao [a], Jianer Zhou [c]

[a] Department of Energy Materials, School of Materials Science and Engineering, Hefei University of Technology, No.193 Tunxi Road, Hefei, Anhui 230009, China
[b] Key Laboratory of Advanced Functional Materials and Devices, School of Materials Science and Engineering, Hefei University of Technology, No.193 Tunxi Road, Hefei, Anhui 230009, China
[c] National Engineering Research Centre for Domestic & Building Ceramics, School of Materials Science and Engineering, Jingdezhen Ceramic Institute, Jingdezhen, Jiangxi 333403, China

HIGHLIGHTS

- CO_2 was electrochemically reduced into CO in H^+-type solid oxide electrolysers.
- LSCM-based oxygen electrode shows excellent performance for H_2O electrolysis.
- Reoxidation of LSCM is the main process at low voltage during electrolysis.
- Electrochemical oxidation of H_2O is main process at high voltage in electrolysis.

ARTICLE INFO

Article history:
Received 30 August 2012
Received in revised form
19 November 2012
Accepted 6 January 2013
Available online 16 January 2013

Keywords:
Solid oxide electrolyser
Steam electrolysis
Carbon dioxide
Proton conductor
Electrochemical reduction

ABSTRACT

In this paper, we demonstrate the direct conversion of CO_2/H_2O into fuel in a proton-conducting solid oxide electrolyser with the configuration $(La_{0.75}Sr_{0.25})_{0.95}Mn_{0.5}Cr_{0.5}O_{3-\delta}$ (LSCM, oxygen electrode)/$BaCe_{0.5}Zr_{0.3}Y_{0.16}Zn_{0.04}O_{3-\delta}$ (BCZYZ, proton-conducting electrolyte)/Ni (fuel electrode) at 600 °C, where 5% H_2O/Ar and 100% CO_2 are fed into the oxygen electrode and fuel electrode, respectively. AC impedance spectroscopy and I–V testing demonstrate two main processes in the electrochemical process from 0 to 2 V: (1) the reoxidation of the LSCM electrode ($Mn^{3\pm} \rightarrow Mn^{4\pm}$) below 1.2 V (iR-corrected voltage) and (2) the oxidation of H_2O ($H_2O - 2e \rightarrow H^{\pm} \pm 1/2O_2$) above 1.2 V (iR-corrected voltage). The current density reaches ~0.1 Acm^{-2} at 2 V versus open circuit voltage (OCV) with a total polarisation resistance of 7.5 Ωcm^2. Steam is steadily electrolysed under a 2 V load at 600 °C, and the generated protons in the fuel electrode are simultaneously and completely utilised to electrochemically reduce CO_2 with 100% selectivity and ~90% current efficiency to CO fuel. However, the carbon deposition, poisoning and oxidation of Ni metal in the fuel electrode degrade the cell performance.

1. Introduction

Growing concerns over the consequences of global climate change are forcing a major shift in the energy portfolio from the current dominance of fossil fuels towards a rich and diverse energy supply based upon renewable and environmentally benign sources. Emerging technologies, e.g., solar cells, represent recent technical breakthroughs in harnessing renewable energy while enabling a decreasing/zero level of carbon emission [1,2]. However, the progressive move to decarbonised and renewable energy forms requires a proper energy carrier. The direct generation of fuels from CO_2/H_2O with renewable electricity has therefore been proposed as an alternative way to transport renewable energy from where it is available to its point of use. The recycling of CO_2 would advance us into a carbon-neutral renewable and sustainable energy cycle. This new fuel production strategy can provide a carbon-neutral renewable energy cycle.

Solid oxide electrolysers have been attracting great interest due to their high efficiency in converting electrical energy into chemical energy [3–5]. They can exploit available heat streams to maximise electrical efficiency and operate at higher temperatures, offering both thermodynamic and kinetic advantages. We have recently demonstrated the successful electrochemical conversion of CO_2/H_2O into synthesis gas as well as synthetic fuel CH_4 in an oxygen-ion-conducting solid oxide electrolyser with the configuration (LSM, oxygen electrode) $(La_{0.8}Sr_{0.2})_{0.95}MnO_{3-\delta}$/YSZ (2 mm-thick oxygen-ion-conducting electrolyte)/$La_{0.2}Sr_{0.8}TiO_{3+\delta}$ (LST, fuel

* Corresponding authors. Department of Energy Materials, School of Materials Science and Engineering, Hefei University of Technology, No.193 Tunxi Road, Hefei, Anhui 230009, China. Tel.: +86 551 2905413.
E-mail addresses: xiekui@hfut.edu.cn (K. Xie), ycwu@hfut.edu.cn (Y. Wu).

0378-7753/$ – see front matter © 2013 Elsevier B.V. All rights reserved.
http://dx.doi.org/10.1016/j.jpowsour.2013.01.039

electrode) [6]. At the fuel electrode, CO_2 and H_2O molecules are electrochemically reduced to CO and H_2, respectively, and O^{2-} ions, which are then transported through the oxygen-ion-conducting electrolyte to the oxygen electrode, where O_2 is released. The hydrogen species produced can further react with the produced CO directly, giving rise to synthetic hydrocarbon fuels in the presence of appropriate metal catalysts. The direct synthesis of fuel from CO_2/H_2O in a single reaction step is a significant advance towards a renewable energy supply with zero carbon dioxide emissions.

In addition to oxygen-ion-conducting solid oxide electrolysers, proton-conducting solid oxide electrolysers have also attracted considerable attention because they are able to operate with high efficiency in conjunction with renewable electricity and to effectively exploit available heat streams (such as exhaust heat from nuclear plants) [7,8]. More importantly, they can efficiently produce pure hydrogen and oxygen through high-temperature steam electrolysis because oxygen and hydrogen are generated in two different electrodes and there is no need to separate them. In a proton-conducting solid oxide electrolyser, steam is electrochemically oxidised at the oxygen electrode in-situ and simultaneously split into oxygen and protons under an external electrolysis potential. Protons diffuse across the proton-conducting electrolyte to the fuel electrode, where the formation of pure hydrogen from protons occurs in the three-phase boundary. This feature makes it possible to utilise the proton before its formation of hydrogen at the cathode three-phase boundary to electrochemically reduce CO_2 into hydrocarbons in the presence of appropriate in-situ metal catalysts under sufficient external loads.

In this paper, we demonstrate the successful in-situ electrochemical conversion of H_2O/CO_2 to fuel in a proton-conducting solid oxide electrolyser, as shown in Fig. 1. The cell employs an electrolyte-supported configuration of $(La_{0.75}Sr_{0.25})_{0.95}Mn_{0.5}Cr_{0.5}O_{3-\delta}$ (LSCM, oxygen electrode)/$BaCe_{0.5}Zr_{0.3}Y_{0.1}6Zn_{0.04}O_{3-\delta}$ (BCZYZ, proton-conducting electrolyte)/Ni (fuel electrode). The oxygen electrode is maintained under strongly oxidising conditions in steam electrolysis, where a pure redox active metal cannot be used. It is therefore necessary to develop an appropriate oxygen electrode with high catalytic activity and low overpotentials. Perovskite $(La_{0.75}Sr_{0.25})_{0.95}Mn_{0.5}Cr_{0.5}O_{3-\delta}$ (LSCM) is an active and redox-stable material that has attracted much attention in SOFCs and is therefore a good oxygen electrode material candidate [9]. Furthermore, the p-type conduction of the LSCM oxygen electrode would correspond well with the oxidising condition in the proton-conducting solid oxide electrolyser and therefore result in better electrode polarisation performance under electrolysis conditions. Perovskite-type ceramic $BaCe_{0.5}Zr_{0.3}Y_{0.16}Zn_{0.04}O_{3-\delta}$ (BCZYZ) is adopted as an electrolyte in this work because it has recently been proven to be an excellent proton conductor with good chemical stability, high proton conductivity and a low sintering temperature [10]. This cell utilises a pre-reduced composite fuel electrode Ni/BCZYZ, where Ni offers electronic conduction and BCZYZ provides proton conductivity. From a thermodynamics viewpoint, a high concentration of the reactant is favourable for positive reaction. Therefore, 100% CO_2 is supplied into the cathode to facilitate the electrochemical reduction.

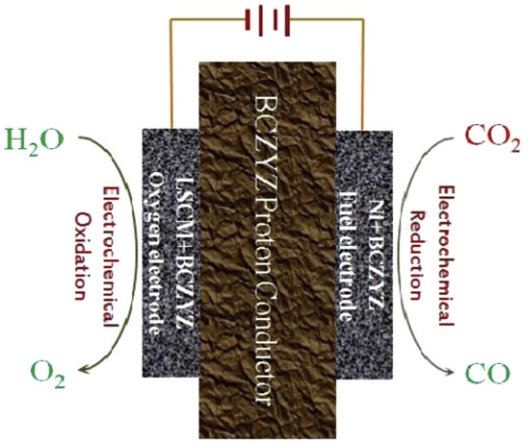

Fig. 1. Schematic of the in-situ electrochemical conversion of H_2O/CO_2 in a proton-conducting solid oxide electrolyser with the configuration $(La_{0.75}Sr_{0.25})_{0.95}Mn_{0.5}Cr_{0.5}O_{3-\delta}$ (LSCM, oxygen electrode)/$BaCe_{0.5}Zr_{0.3}Y_{0.16}Zn_{0.04}O_{3-\delta}$ (BCZYZ, proton-conducting electrolyte)/Ni (fuel electrode). Oxygen electrode: $H_2O - 2e \rightarrow H^{\pm} \pm 1/2O_2$; fuel electrode: $CO_2 \pm 2H^{\pm} \pm 2e \rightarrow CO \pm H_2O$.

2. Experimental

In this work, ceramic proton-conducting electrolyte $BaCe_{0.5}Zr_{0.3}Y_{0.16}Zn_{0.04}O_{3-\delta}$ powders were synthesised by a modified glycine–nitrate process at 1150 °C for 2 h with precursors of $Ba(NO_3)_2$, $Ce(NO_3)_3{\bullet}6H_2O$, $Zr(NO_3)_4{\bullet}6H_2O$, $Y(NO_3)_3{\bullet}6H_2O$ and ZnO. $(La_{0.75}Sr_{0.25})_{0.95}Mn_{0.5}Cr_{0.5}O_{3-\delta}$ (LSCM) powders were prepared with La_2O_3, $Sr(NO_3)_2$, $Cr(NO_3)_3$ and $Mn(NO_3)_2$ in the same way described above, and the final heat treatment is also at 1250 °C for 2 h. X-ray diffraction studies (Stone, CuK_{a1}, Transmitting mode, 2° min^{-1}) were performed to confirm the phase formation of BCZYZ and LSCM. The oxygen electrode powders were prepared by mechanically blending fine BCZYZ powder with LSCM in a 40:60 weight ratio in a mortar. The fuel electrode powders were also prepared by mechanically blending fine BCZYZ powder with green NiO (350 mesh) in a 40:60 weight ratio in a mortar. The 1-mm-thick BCZYZ disc electrolyte support was prepared by dry-pressing BCZYZ powder into a green disk with a diameter of 20 mm followed by a high-temperature sintering in air at 1300 °C for 5 h. The two surfaces of the obtained electrolyte support were mechanically polished with sand paper (1000 mesh), ultrasonically cleaned in ethanol and distilled water several times and dried in air overnight. The oxygen electrode slurry was prepared by directly milling fine BCZYZ powder and LSCM powder in a 40:60 weight ratio in alpha-terpineol with a cellulose additive in a mortar, where the cellulose is utilised to create porosity. The two electrodes were then screen-printed onto an electrolyte in a symmetric position with an area of 1 cm^2 followed by heat treatment at 1150 °C (2 °C min^{-1}) for 3 h in air to assemble a single cell [11]. The current collection layer was constructed with silver paste, which was printed onto both electrode surfaces and fired at 550 °C (3 °C min^{-1}) for 30 min in air. The external circuit was made with silver electrical wire (0.1 mm in diameter), which was then connected to both current collectors using silver paste followed by firing at 550 °C (3 °C min^{-1}) for 30 min in air. The single solid oxide electrolyser was sealed to a homemade testing jig using ceramic paste (AMERCO, Ceram bond 552) for electrochemical measurements. The OCV reached 1.01 V when H_2 was supplied into the fuel electrode with an LSCM-based oxygen electrode exposed to static air. The cell was then electrochemically studied after the reduction of the fuel electrode was complete. The CO_2 and H_2O gas flows were controlled via a mass flow meter and a syringe pump, respectively, for electrochemical reduction and oxidation at 700 °C under external electrical voltages. Electrochemical measurements, including AC impedance, current–voltage (I–V) and open circuit voltage (OCV) measurements, were conducted using a Schlumberger Solartron 1255 Frequency Response Analyser coupled with a 1287 Electrochemical Interface controlled by Zplot Electrochemical Impedance Software. The cathode output gas was connected to a U-type cooling tube in dry ice to eliminate any steam in the mixed gases before being supplied into an online Prolab 300 (Thermoscientific) mass

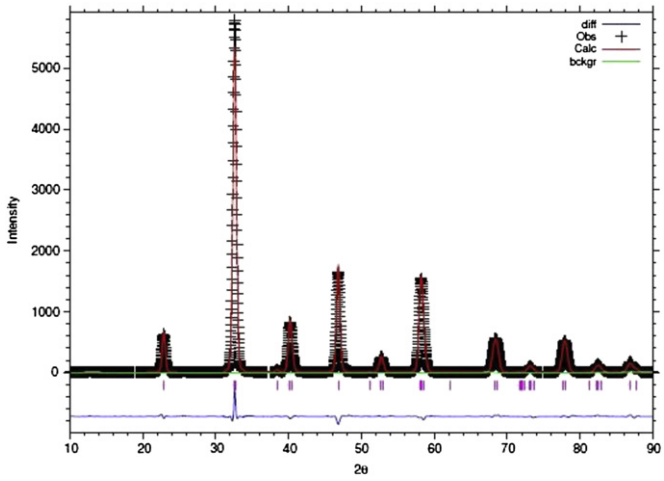

Fig. 2. XRD Rietveld refinement of the oxygen electrode $(La_{0.75}Sr_{0.25})_{0.95}Mn_{0.5}Cr_{0.5}O_{3-\delta}$ (LSCM) prepared at 1250 °C (wR_p = 0.2516, R_p = 0.1352, Chi = 1.558).

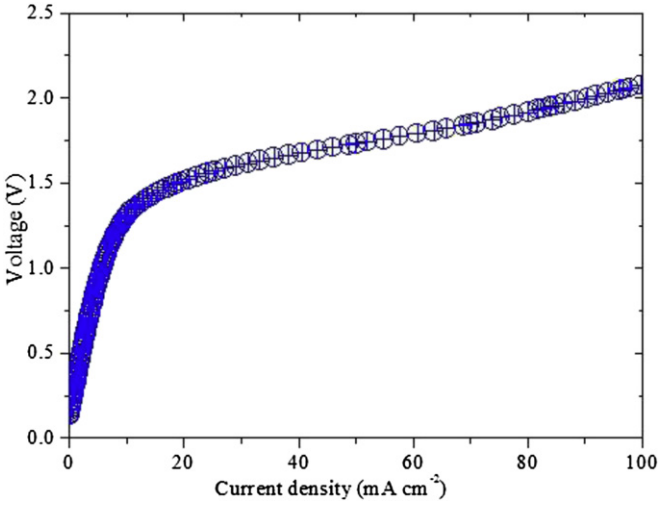

Fig. 4. Current density versus applied voltage of the proton-conducting solid oxide electrolyser for the electrolysis of H_2O and the electrochemical reduction of CO_2 at 600 °C; 5% H_2O/Ar and 100% CO_2 were fed into the oxygen and fuel electrodes, respectively.

spectrometer (MS). The microstructure of the as-prepared electrolyser was characterised using a scanning electron microscope (JEOL 5600) after testing. XPS (X-ray photoelectron spectroscopy) was performed on a Thermo ESCALAB 250 instrument using monochromatised Al Kα at hn ¼ 1486.6 eV to analyse the surface of the fuel electrode after a long-term test.

3. Results and discussion

Fig. 2 shows the XRD Rietveld refinement of the as-prepared $(La_{0.75}Sr_{0.25})_{0.95}Mn_{0.5}Cr_{0.5}O_{3-\delta}$ (LSCM) sample, in which the only strong peaks correspond to the space group R-3c (a = 0.549297 nm, b = 0.549297 nm, c = 1.33416 nm, alpha = 90°, beta = 90°, gamma = 120°). Using the composite oxygen electrode LSCM/BCZYZ and composite fuel electrode NiO/BCZYZ, a single solid oxide electrolyser is constructed based on a BCZYZ proton-conducting electrolyte support (1.0 mm in thickness), and the microstructure is shown in Fig. 3. The two 20-μm-thick porous electrode layers adhere to the electrolyte very well. The porous silver current collector layer is approximately 2 μm in thickness.

Fig. 4 shows the current density as a function of applied voltage (I–V curve) at 600 °C. The open circuit voltage (OCV) of the electrolyser is approximately 1.01 V when the fuel electrode and oxygen electrode are exposed to H_2 and air, respectively, which is consistent with the OCV for a solid oxide fuel cell fuelled with hydrogen. However, when steam is supplied into the oxygen electrode, the OCV dropped significantly to 0.13 V, most likely due to the significant change in oxygen concentration caused by steam splitting at this temperature. In this experiment, the oxygen partial pressure could reach 10^{-5}–10^{-4} atm at such temperatures. Small amounts of H_2 might also be diffusing through microcracks or via ambipolar diffusion, as both holes and protons have some mobility under these conditions, which would further affect the OCVs. As shown in the I–V curve, the relationship between the current and voltage is far from linear. The maximum current density reached 0.1 Acm^{-2} at 2 V, which is approximately 1 V with respect to the open circuit potential for H_2 versus air.

To study the change in cell resistance under different voltages, the dV/dI curves (cell resistance) are plotted versus current density and iR-corrected voltage in Fig. 5 (a) and (b), respectively. The cell resistance dropped significantly below 10 mAcm^{-2}, as shown in Fig. 5(a); however, it is generally stable above this value. Similarly, as shown in Fig. 5(b), a considerable decrease in cell resistance is observed below 1.4 V (iR-corrected voltage), above which the cell resistance does not change. Two different dominant processes might occur from 0 to 2 V for the solid oxide electrolyser at 600 °C. The oxidation of the LSCM oxygen electrode should be the dominant process below 1.2 V (iR-corrected voltage); however, the onset

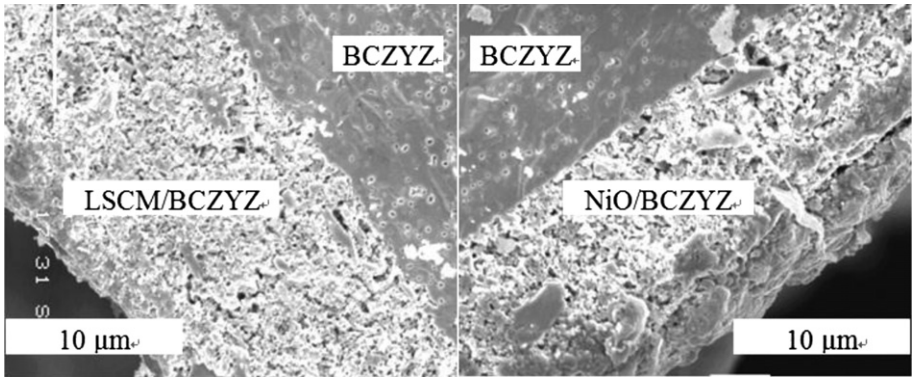

Fig. 3. Microstructure of the solid oxide electrolyser with the configuration $(La_{0.75}Sr_{0.25})_{0.95}Mn_{0.5}Cr_{0.5}O_{3-\delta}$ (LSCM, oxygen electrode)/$BaCe_{0.5}Zr_{0.3}Y_{0.1}6Zn_{0.04}O_{3-\delta}$ (BCZYZ, proton-conducting electrolyte)/Ni (fuel electrode).

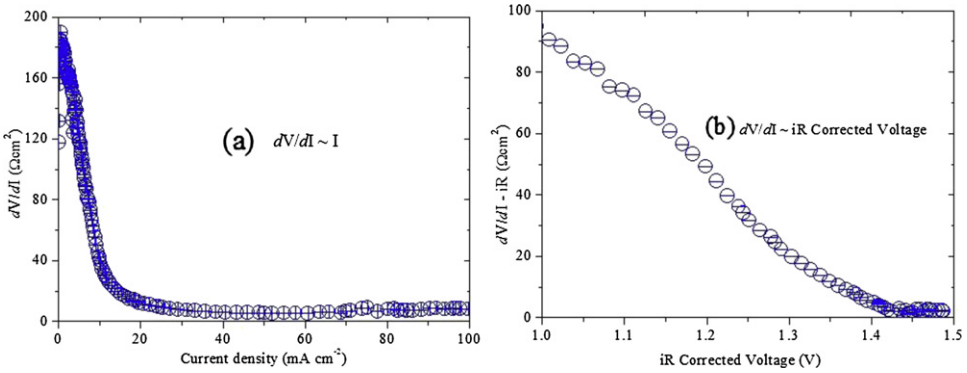

Fig. 5. dV/dI plotted with current density I (a) and iR-corrected voltage V (b), where the data were derived from the I–V curve of the solid oxide electrolyser for H_2O electrolysis and CO_2 reduction at 600 °C; 5% H_2O/Ar and 100% CO_2 were fed into the oxygen and fuel electrodes, respectively.

of steam electrolysis could be anticipated above this voltage, as the OCV of the H_2/O_2 fuel cell is approximately 1.2 V. At high voltages, the oxidation of the LSCM oxygen electrode is sufficient, which leads to a stable cell resistance above 1.4 V (iR-corrected voltage). In-situ AC impedance spectroscopy was therefore performed under different loads to investigate the R_s and R_p changes, where R_s and R_p are the series resistance and electrode polarisations of the cell, respectively.

As shown in Fig. 6, R_s peaks at 1.4 V and then gradually declines by approximately 10% as the voltage increases from 1.4 to 2 V, which may be attributed to the contribution of p-type conduction ($h^\bullet$) caused by the oxidising conditions on the oxygen electrode side. The variation in R_s might also be related to changes in the R_p element affecting the intercept and, particularly for lower R_p values, an enhancement of the lateral conductivity in the oxygen electrode at high potentials. R_p decreased sharply with voltage in the lower-voltage region, whereas R_s dominated the total cell resistance in the high-voltage region, implying that the electrode process is the dominant process at low voltages but that the ion transportation in the electrolyte dominated the entire process at high voltages. To understand the electrode process, the AC impedance data under polarisation at 1.6 V and 2.0 V (iR-corrected: 1.1 V and 1.5 V, respectively) were modelled with an equivalent circuit. The cell

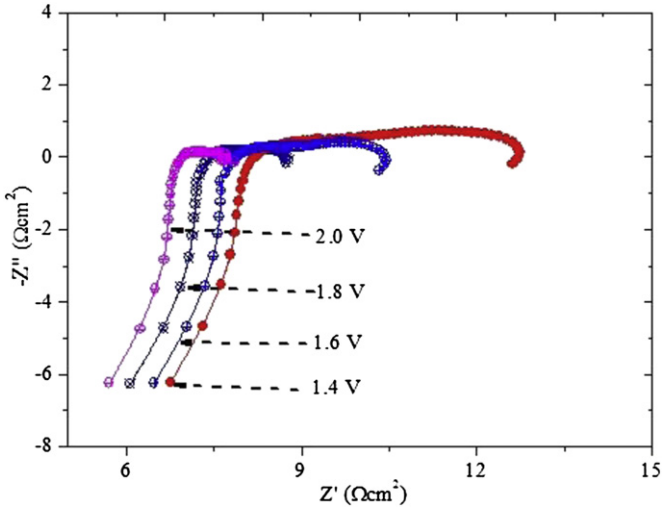

Fig. 6. In-situ AC impedance of the solid oxide electrolyser for the electrolysis of H_2O and the reduction of CO_2 at 600 °C with external applied voltages ranging from 1.4 to 2.0 V versus OCV; 5% H_2O/Ar and 100% CO_2 were fed into the oxygen and fuel electrodes, respectively.

resistance measured by AC methods are slightly lower than those obtained from the gradients of the I–V curves at lower potentials but are consistent with the results from the DC measurements.

As shown in Fig. 7(a), the electrode process is assumed to be comprised of two arcs with an equivalent circuit inserted in the figure. The R_1 value of 2 Ωcm^2 indicates a high-frequency process, which reflects the transport/transfer of oxygen intermediates/oxide ions between LSCM and BCZYZ [12]. In contrast, the R_2 value of 2.4 Ωcm^2 indicates a very clear low-frequency process, especially at low voltages, as the semi-circles shrink with the increase in voltage. The steam splitting at 600 °C produced ~10^{-5}–10^{-4} atm of oxygen partial pressure, which is a moderately reducing condition and certainly reduces the LSCM oxygen electrode. The applied voltage leads to the reoxidation of LSCM below 1.2 V (iR-corrected voltage), which leads to better p-type conductivity for the LSCM oxygen electrode and thereby improves the electrode polarisation. It is therefore believed that the low-frequency process may correspond to the electrochemical process of LSCM reoxidation. At higher voltages, the two arcs are still clear, whereas R_1 and R_2 decreased to 0.6 and 0.6 Ωcm^2, respectively. The significant decrease in R_2 indicates that the oxidation of LSCM is no longer the main limiting process at high voltages. However, the dissociative adsorption, transfer of species at the three-phase boundary and surface diffusion might be limiting at low frequencies and correspond to the low-frequency process.

The Po_2 dependence of oxygen deficiency, δ, in $(La_{0.75}Sr_{0.25})_{0.95}Mn_{0.5}Cr_{0.5}O_{3-\delta}$ plays an important role under reducing conditions due to the $Mn^{3+} \leftrightarrow Mn^{4+}$ transition, which affects the charge carrier. The δ value is generally independent of Po_2 at higher oxygen partial pressures but is strongly related to Po_2 at low oxygen partial pressures. Furthermore, the conductivity of the LSCM varies similarly to δ [13]. The applied voltage in our experiment produces oxidising conditions at the oxygen electrode and therefore plays the same role as Po_2. As the initial potential under the H_2O atmosphere is only 0.13, the LSCM experiences moderately reducing conditions (~ 10^{-5}–10^{-4} atm). Higher voltages lead to reoxidising conditions in the oxygen electrode, which enhances the conductivity of the ceramic. This phenomenon may be the cause of the R_p changes in different voltage regions. In addition, high voltages lead to favourable kinetics for the electrode reaction, which can also improve the electrode polarisation at high voltages.

There are two main electrochemical processes from 0 to 2 V during the steam electrolysis process: the reoxidation of the LSCM anode and the oxidation of H_2O. The LSCM oxidation is the main electrochemical process below 1.2 V (iR-corrected voltage), whereas the oxidation of H_2O to O_2 mainly dominates the electrolysis process at high voltages. Fig. 8 shows the short-term performance for the simultaneous process of steam electrolysis and

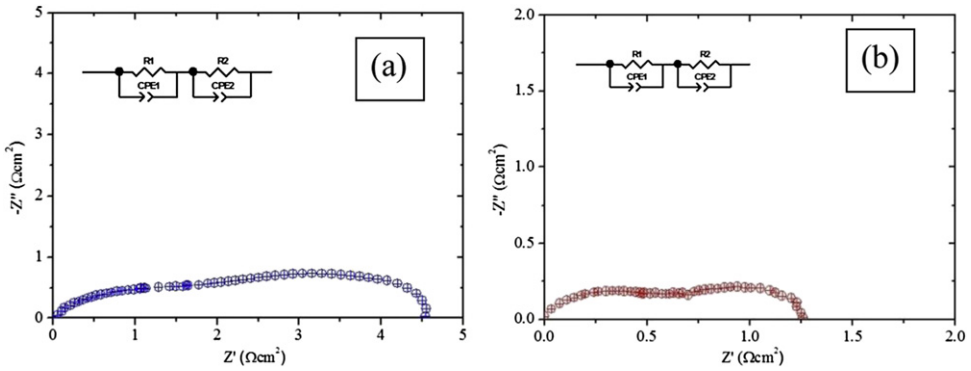

Fig. 7. Model of the in-situ AC impedance of the solid oxide electrolyser for steam electrolysis under (a) 1.4 V and (b) 2.0 V at 600 °C.

CO_2 reduction at 600 °C. The current generally remains constant at 0.1 Acm^{-2} when 2 V is applied for electrolysis, indicating a stable electrochemical process. As shown in Fig. 9, the only fuel, carbon monoxide, from the efficient electrochemical reduction of CO_2 reaches approximately 1.2 ml min cm^{-2} under these conditions, with a current efficiency of ~90%. The loss of current efficiency may be related to the transport of other species in the electrolyte, i.e., oxygen ions and holes. Furthermore, other metal catalysts can be utilised in the fuel electrode to generate other fuels, such as C_2H_6 or CH_3OH. However, in our work, only CO was detected, which might be attributed to the dynamic advantage of the conversion of CO_2 into CO. Organic chemical fuels, such as CH_4, were absent in our work, despite the formation of methane having a thermodynamic advantage.

However, it should be noted that the Ni-based fuel electrode is exposed to a mixture of CO_2, CO and H_2O gases, which might induce the poisoning, carbon deposition and oxidation of the Ni metal. To further to validate the chemical stability of the Ni-based fuel electrode, a long-term test was performed to investigate the degradation of the cell performance. As shown in Fig. 10, the current density decreased continuously with time (15 h) at a static applied potential (2.0 V), which indicates the significant degradation of the cell performance. This degradation is most likely due to a chemical change in the Ni-based fuel electrode during the test. Fig. 11 shows the C and Ni XPS signals for the fuel electrode after the long-term

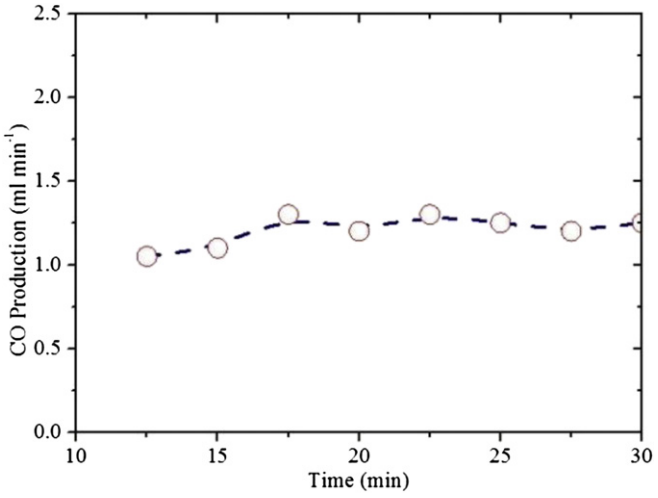

Fig. 9. Short-term performance of the as-prepared solid oxide electrolyser with an applied voltage of 2 V at 600 °C for the electrolysis of H_2O and the reduction of CO_2; the 5% H_2O/Ar and 100% CO_2 were fed into the oxygen and fuel electrodes, respectively.

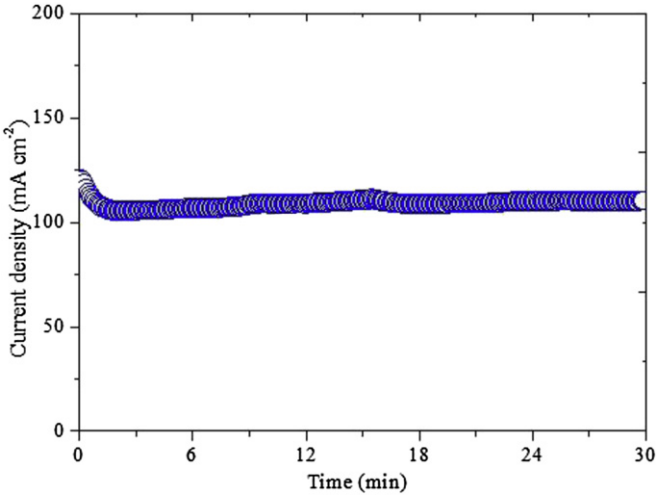

Fig. 8. Short-term performance of the as-prepared solid oxide electrolyser with an applied voltage of 2 V at 600 °C for the electrolysis of H_2O and the reduction of CO_2; 5% H_2O/Ar and 100% CO_2 were fed into the oxygen and fuel electrodes, respectively.

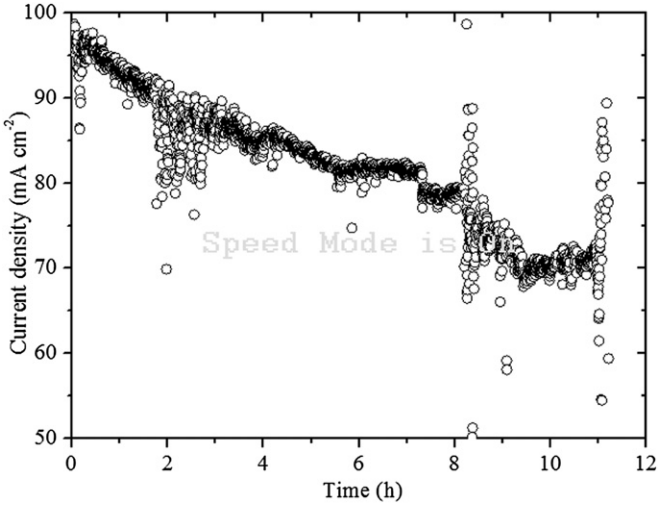

Fig. 10. Long-term performance of the as-prepared solid oxide electrolyser with an applied voltage of 2 V at 600 °C for the electrolysis of H_2O and the reduction of CO_2; 5% H_2O/Ar and 100% CO_2 were fed into the oxygen and fuel electrodes, respectively.

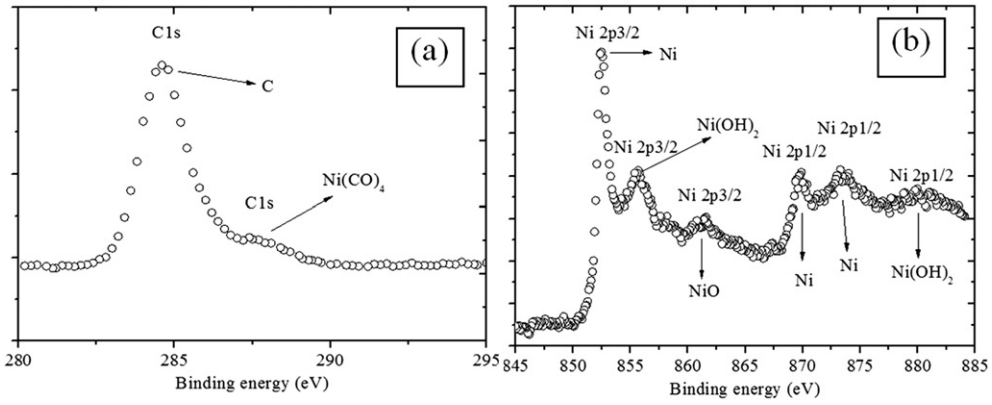

Fig. 11. XPS of the Ni-based fuel electrode of the solid oxide electrolyser after long-term testing.

test. The C signal, as shown in Fig. 11 (a), was observed in the fuel electrode, which implies that the carbon deposition occurs during the electrochemical reduction of CO_2 [14]. In addition, a weak $Ni(CO)_4$ signal was observed, which might be related to the CO poisoning of Ni forming the adsorbed $Ni(CO)_4$ molecules in the fuel electrodes [15]. As shown in Fig. 11 (b), a strong Ni XPS signal was present [16]; however, the NiO and $Ni(OH)_2$ XPS signals are both observed in the fuel electrode [16], which indicates that the Ni metal has been partially oxidised by the produced H_2O at 600 °C. All of these phenomena together lead to the degradation of cell performance during the electrochemical process.

4. Conclusions

In this work, a proton-conducting solid oxide electrolyser with the configuration $(La_{0.75}Sr_{0.25})_{0.95}Mn_{0.5}Cr_{0.5}O_{3-\delta}$ (LSCM, oxygen electrode)/$BaCe_{0.5}Zr_{0.3}Y_{0.1}6Zn_{0.04}O_{3-\delta}$ (BCZYZ, proton-conducting electrolyte)/Ni (fuel electrode) was demonstrated for the efficient conversion of H_2O/CO_2 into fuel at 600 °C. The electrochemical oxidation of the LSCM composite electrode, which might be considered electrode conditioning, mainly dominates the overall cell process at lower voltages according to in-situ impedance spectroscopy. In contrast, the electrochemical conversion of H_2O/CO_2 to produce fuel is the main process at higher voltages. Furthermore, the in-situ electrochemical conversion of CO_2 into CO showed 100% selectivity and 90% current efficiency with the Ni-based fuel electrode. However, the carbon deposition, poisoning and oxidation of Ni metal in the fuel electrode degrade the cell performance. Future work will be performed by developing ceramic fuel electrodes to prevent the carbon deposition, poisoning and oxidation.

Acknowledgements

We would like to acknowledge funding from the NSFC (No. 51142008) for supporting this research.

References

[1] M.I. Hoffert, K. Caldeira, G. Benford, D.R. Criswell, C. Green, H. Herzog, A.K. Jain, H.S. Kheshgi, K.S. Lackner, J.S. Lewis, H.D. Lightfoot, W. Manheimer, J.C. Mankins, M.E. Mauel, L.J. Perkins, M.E. Schlesinger, T. Volk, T.M.L. Wigley, Science 298 (2002) 981.
[2] S. Sista, Z. Hong, L. Chen, Y. Yang, Energy Environ. Sci. 4 (2011) 1606.
[3] X. Yang, J.T.S. Irvine, J. Mater. Chem. 18 (2008) 2349.
[4] K. Xie, Y.Q. Zhang, G.Y. Meng, J.T.S. Irvine, J. Mater. Chem. 21 (2011) 195.
[5] S. Dalgaard Ebbesen, M. Mogensen, J. Power Sources 193 (2009) 349.
[6] K. Xie, Y. Zhang, G. Meng, J.T.S. Irvine, Energy Environ. Sci. 4 (2011) 2218.
[7] P.A. Stuart, T. Unno, J.A. Kilner, S.J. Skinner, Solid State Ionics 179 (2008) 1120.
[8] T. Sakai, S. Matsushita, H. Matsumoto, S. Okada, S. Hashimoto, T. Ishihara, Int. J. Hydrogen Energ. 34 (2009) 56.
[9] S. Tao, J.T.S. Irvine, Nat. Mater. 2 (2003) 320.
[10] S. Tao, J.T.S. Irvine, Adv. Mater. 12 (2006) 1581.
[11] K. Xie, R. Yan, X. Xu, X. Liu, G. Meng, J. Power Sources 187 (2009) 403.
[12] M.J. Jorgensen, M. Mogensen, J. Electrochem. Soc. 148 (2001) A433.
[13] G. Kim, G. Corre, J.T.S. Irvine, J.M. Vohs, R.J. Gorte, Electrochem. Solid-State Lett. 11 (2008) B16.
[14] G. Witek, M. Noeske, G. Mestl, S. Shaikhutdinov, R.J. Behm, Catal. Lett. 37 (1996) 35.
[15] K. Kishi, Y. Motoyoshi, S. Ikeda, Surf. Sci. 105 (1981) 313.
[16] A.N. Mansour, Surf. Sci. Spectra 3 (1994) 211.